

# Dalton Transactions

Accepted Manuscript



This is an *Accepted Manuscript*, which has been through the Royal Society of Chemistry peer review process and has been accepted for publication.

*Accepted Manuscripts* are published online shortly after acceptance, before technical editing, formatting and proof reading. Using this free service, authors can make their results available to the community, in citable form, before we publish the edited article. We will replace this *Accepted Manuscript* with the edited and formatted *Advance Article* as soon as it is available.

You can find more information about *Accepted Manuscripts* in the [Information for Authors](#).

Please note that technical editing may introduce minor changes to the text and/or graphics, which may alter content. The journal's standard [Terms & Conditions](#) and the [Ethical guidelines](#) still apply. In no event shall the Royal Society of Chemistry be held responsible for any errors or omissions in this *Accepted Manuscript* or any consequences arising from the use of any information it contains.

## ARTICLE

# Ultrafast Spectroscopy and Structural Characterization of a Photochromic Isomerizing Ruthenium Bis-sulfoxide Complex

Cite this: DOI: 10.1039/x0xx00000x

Received 00th January 2012,  
Accepted 00th January 2012

DOI: 10.1039/x0xx00000x

[www.rsc.org/](http://www.rsc.org/)Albert W. King,<sup>a</sup> Jason P. Malizia,<sup>a</sup> James T. Engle,<sup>b</sup> Christopher J. Ziegler<sup>b</sup> and Jeffrey J. Rack<sup>a</sup>

Irradiation of  $[\text{Ru}(\text{bpy})_2(\text{bpSOp})](\text{PF}_6)_2$  (where bpy is 2,2'-bipyridine and bpSOp is 1,3-bis(phenylsulfinyl)propane) results in the formation of two new isomers, namely the S,O- and O,O-bonded species. The crystal structure of the *bis*-thioether and *bis*-sulfoxide complexes are reported. NMR spectroscopy of the *bis*-thioether complex in solution is consistent with the molecular structure determined by diffraction methods. Further, NMR spectroscopy of the *bis*-sulfoxide complex reveals two conformers in solution, one that is consistent with the solid state structure and a second conformer showing distortion in the aliphatic portion of the chelate ring. Time-resolved visible absorption spectroscopy reveals isomerization time constants of 91 ps in dichloroethane (DCE) and 229 ps in propylene carbonate (PC). Aggregate isomerization quantum yields of 0.57 and 0.42 have been determined in DCE and in PC, respectively. The kinetics of the thermal reversion from the O,O- to S,O-bonded isomer are strongly solvent dependent, occurring with rates of  $2.41 \times 10^{-3}$  and  $4.39 \times 10^{-5} \text{ s}^{-1}$  in DCE, and  $4.68 \times 10^{-4}$  and  $9.79 \times 10^{-6} \text{ s}^{-1}$  in PC. The two kinetic components are assigned to the two isomers identified in solution.

## Introduction

Photochromic compounds attract the interests of chemists, materials scientists and physicists. The light induced nature of electronic and structural changes in this class generate fascination with regards to how the reaction occurs and to how the changes may be exploited or amplified. For example, computational efforts on photochromic compounds have revealed that isomerization often occurs at a conical intersection or at conical intersection seams.<sup>1-6</sup> These seams are formed at the intersection of at least two electronic surfaces and often involve multiple nuclear coordinates.<sup>7-10</sup> A genuine approach to molecular information storage is through non-linear optical techniques in which efficient light induced refractive index changes can be observed for materials containing sodium nitroprusside ( $\text{Na}_2[\text{Fe}(\text{CN})_5(\text{NO})]$ ). It is manifest that the metastable isomers (O-bonded isonitrosyl, side-on bonded  $\eta^2\text{-NO}$ ) produce the refractive index changes utilized for information storage.<sup>11, 12</sup> There is growing interest in the development of molecular solar-thermal rechargeable batteries based on phototriggered bond-breaking and bond-making properties of photochromic molecules.<sup>13-17</sup> In this approach, solar energy is stored within the chemical bonds of a photochromic material; heat is later released during the exoergodic transformation of the metastable state to the ground

state. Furthermore, a variety of interesting materials comprised of photochromic compounds have been reported and recently reviewed.<sup>18-20</sup> Of special mention are those that result in macroscopic deformations upon irradiation in crystals, elastomers or films.<sup>21-26</sup>

Despite these compelling reports, there are relatively few classes of photochromic compounds.<sup>27</sup> We have designed and created a class of ruthenium polypyridyl sulfoxide photochromes based on phototriggered S $\rightarrow$ O and O $\rightarrow$ S isomerization.<sup>28-30</sup> Recently, we have studied the photophysical and photochemical properties of *bis*-sulfoxide complexes in order to learn the relationship of one isomerization event on the neighboring sulfoxide.<sup>31-33</sup> Our fundamental motivation is to understand the coupling of nuclear movements with the excited state electronic wave function. Here, we report our latest findings on a complex containing an *n*-propyl linker between two sulfoxides. Solvent dependent isomerization is observed in propylene carbonate and 1,2-dichloroethane in both excited state and ground state transformations. Also, a comparative study suggests that rotation within the chelating linker is an important feature of isomerization.

## Experimental

### Materials

Thiophenol was obtained from TCI America, Inc. 1,3-dibromopropane, 2,2'-bipyridyl, *meta*-chloroperoxybenzoic acid (*m*-cpba), ammonium hexafluorophosphate and HPLC-grade propylene carbonate (PC; used as received), were purchased from Sigma-Aldrich. Ruthenium (III) chloride was purchased from Strem and the starting complex Ru(bpy)<sub>2</sub>Cl<sub>2</sub>·2H<sub>2</sub>O was produced in accord with the literature procedure.<sup>34</sup> Potassium hydroxide was purchased from Fisher Scientific, as were all remaining solvents, which were used as received unless otherwise noted.

### Syntheses.

**1,3-bis(phenylsulfanyl)propane (btp).** A solution of potassium hydroxide (1.898 g, 33.8 mmol) and thiophenol (3.30 mL, 32.3 mmol) in 30 mL of ethanol was refluxed for 30 minutes. A solution of 1,3-dibromopropane (1.5 mL, 14.7 mol) in 15 mL of ethanol was added dropwise, after which refluxing was resumed for 6 hours. Solid potassium bromide was filtered with a medium frit and ethanol was removed from the filtrate via rotary evaporation. The residual oil was dissolved in 10 mL of 1,2-dichloroethane (DCE) and washed once with 15 mL of a 1 M solution of potassium hydroxide, followed by 15 mL of ultrapure (18.2 MΩ cm<sup>-1</sup>) water. Solvent was removed from the organic phase via rotary evaporation to yield btp as a colorless, clear liquid. (3.701 mg, 96.7% yield). <sup>1</sup>H NMR (*d*<sub>6</sub>-acetone, 300 MHz): δ (ppm) = 7.36 (m, 8 H), 7.22 (t, 2 H), 3.15 (t, 4 H), 1.97 (m, 2 H).

**[Ru(bpy)<sub>2</sub>(btp)](PF<sub>6</sub>)<sub>2</sub>.** A solution of Ru(bpy)<sub>2</sub>Cl<sub>2</sub>·2H<sub>2</sub>O (0.597 g, 1.14 mmol), silver hexafluorophosphate (0.726 g, 2.87 mmol), and btp (0.315 g, 1.15 mmol) were mixed in 15 mL of deaerated DCE and refluxed under nitrogen for 3 hours. Then, additional silver hexafluorophosphate (0.290 g, 1.14 mmol) and btp (0.079 g, 0.29 mmol) were added to the solution. The reaction was allowed to continue at reflux for an additional 6 hours. After cooling, the reaction mixture was placed in a freezer for 2 hours to precipitate silver chloride, which was subsequently filtered with a fine frit. The resulting filtrate was dried via rotary evaporation. A minimal amount of methanol was employed to dissolve the obtained solid, which was then added dropwise to a concentrated solution of ammonium hexafluorophosphate in ultrapure water (~15 mL). A yellow-orange precipitate formed, which was filtered and washed with two 10 mL portions of water, followed by two 10 mL portions of diethyl ether. The resulting solid as subsequently dissolved in a small volume of acetonitrile and re-precipitated by the addition of an excess of diethyl ether. The resulting precipitate was filtered with a medium frit, washed with two 10 mL portions of a 3:1 diethyl ether:chloroform mixture, and finally washed with two 10 mL portions of diethyl ether. The solid was dried *in vacuo* to give [Ru(bpy)<sub>2</sub>(btp)](PF<sub>6</sub>)<sub>2</sub> as a yellow powder. Alternatively, to facilitate crystallization, the tetrafluoroborate salt has been synthesized in an identical manner, with the exception of using AgBF<sub>4</sub> in place of AgPF<sub>6</sub>. (0.966 g, 89.8% yield). UV-Vis (PC): λ<sub>max</sub> = 414 nm (7000 M<sup>-1</sup>cm<sup>-1</sup>). Emission (77 K, 4:1 EtOH:MeOH) λ<sub>EM</sub> = 600 nm. <sup>1</sup>H NMR (*d*<sub>3</sub>-acetonitrile, 300

MHz): δ (ppm) = 9.87 (d, 2 H), 8.19 (t, 2 H), 7.98 (m, 4 H), 7.68 (t, 4 H), 7.39 (d, 2 H), 7.14 (t, 4 H), 6.79 (t, 4 H), 6.33 (d, 4 H), 3.38 (m, 4 H), 2.73 (m, 2 H). Elemental Analysis: Calculated for [Ru(C<sub>10</sub>H<sub>8</sub>N<sub>2</sub>)<sub>2</sub>(C<sub>15</sub>H<sub>16</sub>S<sub>2</sub>)](PF<sub>6</sub>)<sub>2</sub>·NH<sub>4</sub>PF<sub>6</sub>: C, 37.30%; H, 3.22%; N, 6.22%. Found: C, 37.07%; H, 3.12%; N, 6.01%.

**[Ru(bpy)<sub>2</sub>(bpSop)](PF<sub>6</sub>)<sub>2</sub>.** A solution of [Ru(bpy)<sub>2</sub>(btp)](PF<sub>6</sub>)<sub>2</sub> (0.250 g, 0.26 mmol) and *m*-cpba (~75%, 0.239 g, 1.04 mmol) in 25 mL of acetonitrile was allowed to react at ~5 °C for 4 days. The solution was concentrated to approximately 3 mL via rotary evaporation, taking care not to heat the solution above 30 °C. A solid was precipitated with the addition of ~25 mL of diethyl ether. The resultant solid was filtered with a medium frit and the pale yellow filtrate was washed five times with 5 mL of diethyl ether to give [Ru(bpy)<sub>2</sub>(bpSop)](PF<sub>6</sub>)<sub>2</sub> as a pale yellow powder. To produce the tetrafluoroborate salt, [Ru(bpy)<sub>2</sub>(btp)](BF<sub>4</sub>)<sub>2</sub> is simply used in place of [Ru(bpy)<sub>2</sub>(btp)](PF<sub>6</sub>)<sub>2</sub>. (0.255 g, 98.7% yield). UV-Vis (PC) λ<sub>max</sub> = 345 nm (5500 M<sup>-1</sup>cm<sup>-1</sup>). Emission (77 K, 4:1 EtOH:MeOH) λ<sub>EM</sub> = 457 nm. <sup>1</sup>H NMR (*d*<sub>3</sub>-acetonitrile, 300 MHz): δ (ppm) = 10.24 (d, 2 H), 8.24 (t, 2 H), 8.03 (d, 4 H), 7.81 (t, 4 H), 7.30 (m, 4 H), 7.22 (m, 2 H), 7.01 (t, 4 H), 6.59 (d, 4 H), 4.24 (m, 2 H), 3.97 (m, 2 H), 3.14 (m, 2 H). Elemental Analysis: Calculated for [Ru(C<sub>10</sub>H<sub>8</sub>N<sub>2</sub>)<sub>2</sub>(C<sub>15</sub>H<sub>16</sub>O<sub>2</sub>S<sub>2</sub>)](PF<sub>6</sub>)<sub>2</sub>·2H<sub>2</sub>O: C, 40.64%; H, 3.52%; N, 5.43%. Found: C, 40.53%; H, 3.31%; N, 5.58%.

### Instrumentation.

One- and two-dimensional NMR spectra were collected on a 300 MHz Bruker AG Spectrometer. All spectra are calibrated to residual signal in the deuterated solvent. Fits of <sup>1</sup>H NMR spectra were performed using SpinWorks 3 version 3.1.8.1. Elemental analysis was performed by Atlantic Microlab, Inc. of Norcross, GA, USA. Single crystal X-ray diffraction data were collected at 100 K (Bruker KRYOFLEX) on a Bruker SMART APEX CCD-based X-ray diffractometer system equipped with a Mo-target X-ray tube (λ = 0.71073 Å). The detector was placed at a distance of 5.009 cm from the crystal. Crystals were placed in paratone oil upon removal from the mother liquor and mounted on a plastic loop in the oil. Integration and refinement of crystal data were done using Bruker SAINT software package and Bruker SHELXTL (version 6.1) software package, respectively. Absorption correction was completed by using the SADABS program. UV-Visible spectra, including bulk photolysis and thermal reversion spectra, were collected on an Agilent 8453 UV-Visible Spectrometer. Kinetic fits of UV-Visible data were determined using Origin Pro 8SR0 version 8.0724. All data were collected in propylene carbonate or 1,2-dichloroethane (DCE) deaerated with nitrogen. Irradiation was performed using a Nd:YAG Continuum SURELITE laser pulsing 355 nm at 10 Hz. Briefly, transient absorption data were collected using an Ultrafast Systems, LLC HELIOS spectrometer. The pump beam was generated by a Light Conversion, Ltd TOPAS-C, while the white light continuum probe beam was generated by passing an 800 nm pulse through a CaF<sub>2</sub> crystal. Both beams were pumped by a Spectra-Physics Solstice comprised of a one-box regenerative amplifier, Mai

Tai fs oscillator and an Empower pump laser. Solutions were prepared with an absorption of  $\sim 0.3$  AU, deaerated with nitrogen and pumped in a flow cell at a rate of  $\sim 7$  mL/min. Transient absorption data were corrected by background subtraction, chirp and  $t_0$  correction and subsequently fit using the program Surface Explorer Pro 1.1.5 by Ultrafast Systems

## Results and Discussion

### A. Structural Characterization

The crystal structures of  $[\text{Ru}(\text{bpy})_2(\text{btp})]^{2+}$  and  $[\text{Ru}(\text{bpy})_2(\text{bpSO})]^{2+}$  are shown in Figure 1. Two enantiomers are observed in the unit cell of  $[\text{Ru}(\text{bpy})_2(\text{btp})]^{2+}$  ( $z = 4$ ; space group  $P2(1)$ ) and one in the unit cell of  $[\text{Ru}(\text{bpy})_2(\text{bpSO})]^{2+}$  ( $z = 8$ ; space group  $Fdd2$ ). Select bond distances and angles are displayed in Table 1, with crystallographic data shown in Table S1. Both the thioether and sulfoxide molecules are  $C_2$  symmetric ( $z$ -axis bisecting the S-Ru-S chelate angle) in the solid state. The sulfoxide complex features a short Ru-S bond distance (2.280(1) Å) in comparison to the thioether complex (2.386(2) and 2.371(2) Å). The S=O bond distance in the sulfoxide complex is  $\sim 1.48$  Å, as is commonly observed in coordinated ruthenium sulfoxide complexes. Intramolecular  $\pi$ -stacking between the phenyl and bipyridine rings is observed in both  $[\text{Ru}(\text{bpy})_2(\text{btp})]^{2+}$  and  $[\text{Ru}(\text{bpy})_2(\text{bpSO})]^{2+}$ , with distances of  $\sim 3.65$  and  $\sim 3.29$  Å in the thioether complex and a distance of  $\sim 3.43$  Å in the sulfoxide complex. (Relevant atom and centroid labels are found in the Supporting Information.) The bite angles of the thioether (88.38(5) °) and sulfoxide (88.84(3) °) ligands differ significantly from other reported ruthenium complexes.<sup>35</sup> For example, in  $[\text{Ru}(\text{bpy})_2(\text{OSSO})]^{2+}$  (OSSO is dimethylbis(methylsulfinylmethyl)silane), another six-membered chelating *bis*-sulfoxide complex, the observed bite angle is 92.92(4) °.<sup>33</sup> The bite angle in the five-membered analogue of  $[\text{Ru}(\text{bpy})_2(\text{bpSO})]^{2+}$ ,  $[\text{Ru}(\text{bpy})_2(\text{bpSO})]^{2+}$  (bpSO is 1,2-bis(phenylsulfinyl)ethane), is 85.91(6) °.<sup>32</sup> The most acute of these angles corresponds to the shortest Ru-S bond distance,  $\sim 2.25$  Å in  $[\text{Ru}(\text{bpy})_2(\text{bpSO})]^{2+}$ , while the greatest angle corresponds to the longest bond distance of  $\sim 2.29$  Å, observed in  $[\text{Ru}(\text{bpy})_2(\text{OSSO})]^{2+}$ . As the bite angle reflects the orbital overlap between the ruthenium center and the sulfoxide ligand, this trend implies a relationship between chelate bite angle and the electronic properties of the molecule, though their affect on excited state isomerization dynamics may not be directly predicted.

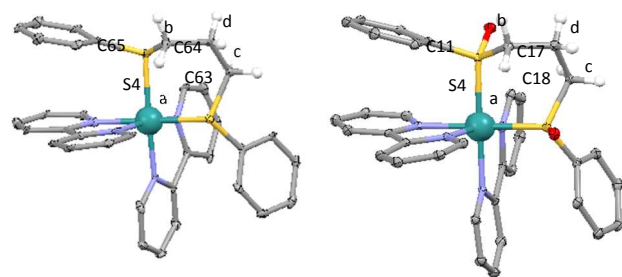


Figure 1. Molecular structures of  $[\text{Ru}(\text{bpy})_2(\text{btp})]^{2+}$  (left) and  $[\text{Ru}(\text{bpy})_2(\text{bpSO})]^{2+}$  (right). Hydrogen atoms have been omitted for clarity and thermal ellipsoids are shown at 30% probability; Ru is rendered as ball.

Both  $[\text{Ru}(\text{bpy})_2(\text{btp})]^{2+}$  and  $[\text{Ru}(\text{bpy})_2(\text{bpSO})]^{2+}$  have been characterized by one- and two-dimensional  $^1\text{H}$  NMR spectroscopy (Figures S1-S9). For the thioether complex, the aromatic (bpy and btp ligands) and aliphatic (propyl bridge) regions of the spectrum exhibit a single set of resonances, indicating that the molecule is  $C_2$  symmetric in solution, consistent with X-ray structural data. The resonances corresponding to the propyl-bridge of the btp ligand are complicated by higher order coupling among the two pair of diastereotopic protons ( $\alpha$  to either S atom) and the central methylene (Figures S1 and S2). Structural characterization of the propyl-bridge in the solution structure is consistent with the solid state structure as determined by X-ray crystallography, as discussed below.

Table 1. Selected Bond Distances (Å) and Angles (deg).

|          | $[\text{Ru}(\text{bpy})_2(\text{btp})](\text{PF}_6)_2$ | $[\text{Ru}(\text{bpy})_2(\text{bpSO})](\text{BF}_4)_2$ |
|----------|--|---|
| Ru-S1    | 2.386(2)   | 2.280(1)  |
| Ru-S2    | 2.371(2)   | 2.280(1)  |
| Ru-N1    | 2.064(4)   | 2.103(2)  |
| Ru-N2    | 2.091(4)   | 2.090(2)  |
| Ru-N3    | 2.075(4)   | 2.103(2)  |
| Ru-N4    | 2.068(5)   | 2.090(2)  |
| S1-O1    | -  | 1.483(2)  |
| S2-O2    | -  | 1.482(2)  |
| N1-Ru-N2 | 79.3(2)  | 78.93(8)  |
| N3-Ru-N4 | 78.2(2)  | 78.93(8)  |
| S1-Ru-S2 | 88.38(5)   | 88.84(3)  |

For the sulfoxide complex, the NMR spectra reveal the presence of two isomers, termed major (M) and minor (m), in a ratio of 1:0.08, assuming the minor isomer to be non- $C_2$  symmetric (see below). The aromatic region is ascribed to the H atoms on the bpy ligands and on the phenyl rings of the bpSO ligand, while the aliphatic region corresponds to H atoms on the propyl bridge (Figure 2). In the aliphatic region, the observed splitting pattern of the propyl bridge for both major and minor isomers (and for the thioether complex) has been simulated using SpinWorks 3 (version 3.1.8.1) to determine the  $J$  coupling constants among the protons of the bridge. In addition to describing the structure of the chelate ring *in situ*, this approach is further useful to differentiate the major and minor isomeric species observed in the sulfoxide complex. With this strategy, we can only simulate resonances associated

with one isomer at a time. Thus, in our simulation of the major isomer, peaks ascribed to the minor isomer are absent, and vice versa. This is manifest in Figure 2, where the simulations and experimental spectra of the aliphatic region are plotted. The  $^2J_{\text{H-H}}$  and  $^3J_{\text{H-H}}$  constants (and resultant angles) extracted from this fitting are shown in Table 2. Detailed discussion of the fitting procedure and specific atom labelling is found in the Supporting Information. Due to the symmetry of the complex, the coupling constants between protons  $\text{H}_a$  and  $\text{H}_b$  (*i.e.*, the diastereotopic pair) are identical to those of the remaining diastereotopic pair for the major isomer. The simulated spectra are in excellent agreement with the experimental data, though it is worth noting that the full quartet observed in the minor sulfoxide isomer at 3.10 ppm is largely occluded by the resonance of the central methylene belonging to the major species. Similar overlap occurs in the case of a triplet observed at 4.09 ppm. The optimization of every other fit parameter, and consistency between the crystal structure and the major isomer however, support the model. The  $J$  coupling constants obtained from the NMR spectral fits may be applied in the Karplus equation to calculate dihedral angles of the aliphatic (propyl-bridging) protons in solution. This allows for comparison between the solution and solid state structure, and further characterization of the two isomers observed in the sulfoxide NMR spectrum. The dihedral angles obtained from this analysis are in good agreement (see Table 2) with those in the crystal structure. The coupling constants describing the major species in the sulfoxide spectrum are similar to those of the thioether complex and are again consistent with those found in the solid state. Calculated dihedral angles of the minor sulfoxide isomer indicate a dramatically different conformation in the propyl-bridge compared to the thioether complex. The angles obtained for the minor species suggest a structure where  $\text{H}_a$  and  $\text{H}_c$ , and  $\text{H}_b$  and  $\text{H}_d$ , are nearly eclipsed, when viewed down a  $\text{C}17\text{--C}18$  axis of the propyl bridge. The structural difference between the major and minor isomer is reminiscent of the staggered and eclipsed conformation of ethane (considering just  $\text{C}17$  and  $\text{C}18$ ). Despite these structural differences, there is no clear evidence of differing photochemistry between the isomers, though we do see differences in the ground state kinetics (see below).

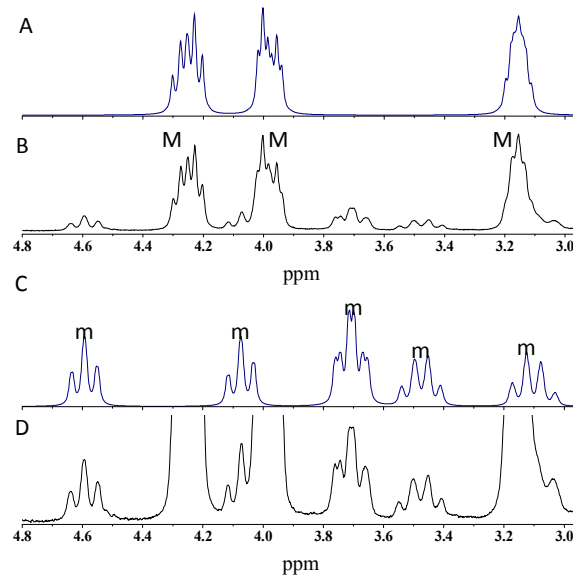


Figure 2. Simulated (A and C) and experimental (B and D) NMR spectra in  $\text{CD}_3\text{CN}$  of major (M; spectra A and B) and minor (m; spectra C and D) isomers of  $\text{S,S-}[\text{Ru}(\text{bpy})_2(\text{bpSOp})]^{2+}$  in the aliphatic region displaying resonances of the propyl bridge.

Table 2 Calculated  $^2J_{\text{H-H}}$  and  $^3J_{\text{H-H}}$  Coupling Constants (Hz) and corresponding angles ( $^\circ$ ) for  $[\text{Ru}(\text{bpy})_2(\text{L})]^{2+}$ , L is btp or bpSOp.

|                                  | $\text{H}_a\text{-H}_b$ | $\text{H}_a\text{-H}_c$ | $\text{H}_a\text{-H}_d$ | $\text{H}_b\text{-H}_c$ | $\text{H}_b\text{-H}_d$ | $\text{H}_c\text{-H}_d$ |
|----------------------------------|-------------------------|-------------------------|-------------------------|-------------------------|-------------------------|-------------------------|
| $J_{\text{H-H}}$ (btp)           | -12.6                   | 5.8                     | 11.2                    | 3.0                     | 6.7                     | -12.6                   |
| Angle (btp) (solution)           | -                       | -46                     | -158                    | 60                      | -41                     | -                       |
| Angle (btp) (crystal)            | 108.1(5)                | -42.2(6)                | -157.3(5)               | 76.3(6)                 | -38.8(7)                | 107.1(5)                |
| $J_{\text{H-H}}$ (bpSOp) (Major) | -13.9                   | 5.5                     | 10.4                    | 10.4                    | 7                       | -13.7                   |
| Angle (bpSOp) (solution)         | -                       | -47                     | -153                    | 60                      | -39                     | -                       |
| Angle (bpSOp) (crystal)          | 108.1(2)                | -41.9(4)                | -157.7(3)               | 76.9(4)                 | -38.9(4)                | 107.4(4)                |
| $J_{\text{H-H}}$ (bpSOp) (Minor) | -13.5                   | 12.0                    | 2.5                     | 2.0                     | 14.0                    | -15.0                   |
| Angle (bpSOp) (solution)         | -                       | -4                      | -111                    | 110                     | 0                       | -                       |

## B. Electronic Spectroscopy

Characteristic of ruthenium polypyridyl dithioether complexes,  $[\text{Ru}(\text{bpy})_2(\text{bptp})](\text{PF}_6)_2$  exhibits a broad absorption band (Figure S10) in the visible spectrum, centered at 414 nm and attributed to a Ru  $d\pi \rightarrow \text{bpy} \pi^*$  metal-to-ligand charge transfer (MLCT) transition. Upon oxidation to the sulfoxide complex,  $\text{S,S-}[\text{Ru}(\text{bpy})_2(\text{bpSO})]^{2+}$ , the MLCT band (Figures 3A, 3B) is observed near 345 nm in PC and 349 nm in DCE, and is slightly obscured by an intense interligand  $\text{bpy} \pi \rightarrow \pi^*$  transition at higher energy. The ground state absorption spectrum of  $\text{S,S-}[\text{Ru}(\text{bpy})_2(\text{bpSO})]^{2+}$  is consistent with those of previously reported S-bonded *bis*-sulfoxide complexes, namely  $[\text{Ru}(\text{bpy})_2(\text{dmsO})_2]^{2+}$  (dmsO is dimethyl sulfoxide),<sup>36</sup>  $[\text{Ru}(\text{bpy})_2(\text{bpSO})]^{2+}$  (bpSO is 1,2-bis(phenylsulfinyl)ethane)<sup>32</sup> and  $[\text{Ru}(\text{bpy})_2(\text{OSSO})]^{2+}$  (OSSO is dimethylbis(methylsulfinylmethyl)silane),<sup>33</sup> which exhibit absorption maxima at 348, 335 and 350 nm, respectively.

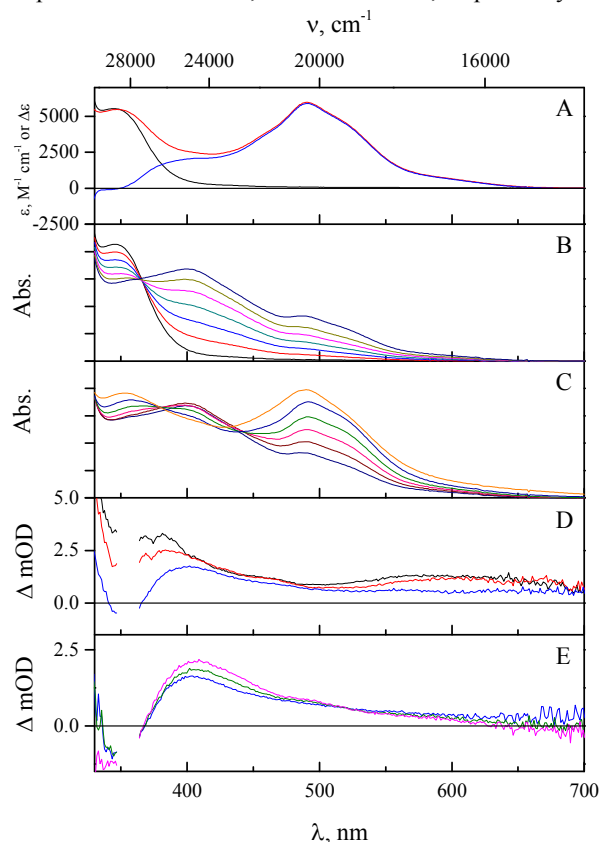


Figure 3. UV-visible and transient absorption spectra in propylene carbonate. A) Electronic spectra of  $\text{S,S-}[\text{Ru}(\text{bpy})_2(\text{bpSO})]^{2+}$  (black), bulk photolysis product  $\text{O,O-}[\text{Ru}(\text{bpy})_2(\text{bpSO})]^{2+}$  (red), and difference (photoproduct –  $\text{S,S}$ ) (blue). B) UV-visible spectra from bulk photolysis obtained at 0 (black,  $\text{S,S}$ -isomer), 1, 2, 4, 6, 9, and 15 min (dark blue). C) UV-visible spectra from bulk photolysis obtained sequentially at 15 (dark blue) 24, 38, 60, 107, and 189 min (orange). D) Transient absorption spectra obtained from pump–probe delays of 0.6 (black), 1 (red) and 30 (blue) ps. E) Transient absorption spectra obtained at pump–probe delays of 30 (blue), 100 (green) and 500 (magenta) ps.

Bulk photolysis of the ground state *bis*-sulfoxide complex with 365 nm light in propylene carbonate yields significant changes in the electronic absorption spectrum (Figures 3A, B, & C) that are consistent with  $\text{S} \rightarrow \text{O}$  isomerization of each sulfoxide. Initially, a broad band forms near 400 nm and develops into a

distinct peak centered at 405 nm, while an isosbestic point emerges at 366 nm (Figure 3B). Upon continued irradiation, the 405 nm feature loses intensity and two new bands appear at 353 and 492 nm (Figure 3C). Concomitant with these changes, the isosbestic point at 366 nm is lost and a new isosbestic point develops at 380 nm during the latter transformation. The photostationary spectrum is reminiscent of the electronic absorption spectrum of  $[\text{Ru}(\text{bpy})_2(\text{H}_2\text{O})_2]^{2+}$  (where the lowest energy absorption maximum occurs at 490 nm),<sup>37</sup> and of that observed in the O,O-bonded isomers of  $[\text{Ru}(\text{bpy})_2(\text{dmsO})_2]^{2+}$ ,  $[\text{Ru}(\text{bpy})_2(\text{bpSO})]^{2+}$  and  $[\text{Ru}(\text{bpy})_2(\text{OSSO})]^{2+}$ .<sup>31, 32, 36, 38</sup> The sequential nature of the spectral changes are suggestive of two successive isomerizations, where a first isomerization yields an S,O-bonded isomer and a second isomerization produces an O,O-bonded isomer from the S,O-isomer. Indeed, we observed similar bulk spectral changes in our study of  $[\text{Ru}(\text{bpy})_2(\text{bpSO})]^{2+}$ .<sup>32</sup> Also, such an S,O-bonded structure is stable in  $[\text{Os}(\text{bpy})_2(\text{dmsO})_2]^{2+}$  (dmsO is dimethyl sulfoxide), where only a single sulfoxide isomerizes and the absorption maximum of the S,O-bonded isomer is 403 nm.<sup>39</sup> Thus, the 405 nm absorption feature is consistent with an S,O-bonded complex. Notably, loss of the 366 nm isosbestic point and formation of a new isosbestic point at 380 nm in later spectra, concomitant with the loss of the S,O-bonded absorption feature, implies that the final species in the photostationary spectrum is formed directly from an intermediate S,O-bonded isomer. The aggregate isomerization quantum yield,  $\Phi_{\text{S,S} \rightarrow \text{P}}$  (P is photoproduct) is 0.42(5) in PC, as determined by ferrioxalate actinometry. Details of this experiment are included in the Supporting Information. The initial (black) and final bulk photolysis (red) spectra are displayed in Figure 3A.

Importantly, the concentration of  $\text{S,O-}[\text{Ru}(\text{bpy})_2(\text{bpSO})]^{2+}$  increases in the evolution of the bulk photolysis spectra and the S,O-isomer dominates the absorption spectrum prior to the subsequent formation of the O,O-isomer. Accordingly, the quantum yield for the formation of the S,O-bonded complex from the S,S-bonded complex must be greater than the quantum yield for the reaction of the S,O- to yield O,O-isomer. While spectral overlap between the isomers prevents reliable determination of quantum yields for the respective S,S to S,O and S,O to O,O isomerizations, the previously reported  $[\text{Ru}(\text{bpy})_2(\text{bpSO})]^{2+}$  complex exhibits less significant contributions from the S,O-bonded intermediate in the bulk irradiation spectra and never dominates the absorption spectrum. In comparison, this observation suggests that the quantum yield of isomerization for the S,S to S,O isomerization in  $[\text{Ru}(\text{bpy})_2(\text{bpSO})]^{2+}$  is at least comparable to that of the S,O to O,O quantum yield, as the intermediate is apparently never the predominant feature in the spectra and must be consumed soon after it is formed. The S,O intermediate is less reactive in the propyl-bridged complex – which features a seven-membered chelating ring – than in the ethyl-bridged complex, which features a six-membered chelate in the S,O-isomer. Bulk photolysis spectra of  $\text{S,S-}[\text{Ru}(\text{bpy})_2(\text{bpSO})]^{2+}$  in DCE (Figures 4A, B, & C) are in significant contrast to those observed in PC. Short irradiation times at 365 nm yield a rise in

absorption between 400 and ~500 nm, concomitant with a decrease near 350 nm (the S,S-isomer absorption maximum). No distinct peak is initially observed, though broad features are present around 425 and 500 nm (Figure 4B). Continued irradiation yields a general blue-shift of the 425 nm feature toward 408 nm. Ultimately, the feature near 500 nm decays and the peak at 408 nm continues to gain intensity, while shifting further to 400 nm. A new isosbestic point is formed at 416 nm until the spectrum no longer changes with continued irradiation (Figure 4C). It is striking that long irradiation times do not produce an absorption feature near 500 nm, indicative of a *bis*-O,O-isomer. As in PC, the species with a distinct absorption peak about 400 nm is assigned to S,O-[Ru(bpy)<sub>2</sub>(bpSOp)]<sup>2+</sup>. The species which contributes to the transient absorbance near 500 nm is assigned to the O,O-bonded isomer. The aggregate quantum yield for the observed changes as monitored at 400 nm is 0.57(2) in DCE. Unlike in PC, the O,O-bonded isomer never predominates the absorption spectrum and is apparently never present as the primary isomeric photoproduct. The O,O-bonded isomer (featuring an eight-membered chelate ring) must therefore be thermally unstable in DCE, with a reversion rate substantially greater than that of the S,O to O,O photoisomerization quantum yield, and/or there exists a photochemical pathway (O,O to S,O) with a quantum yield greater than that of the S,O to O,O photoisomerization quantum yield (see below). In the case of either explanation, it is surprising that the seemingly minor change in solvent leads to such a dramatic change in reactivity regarding the O,O-bonded isomer.

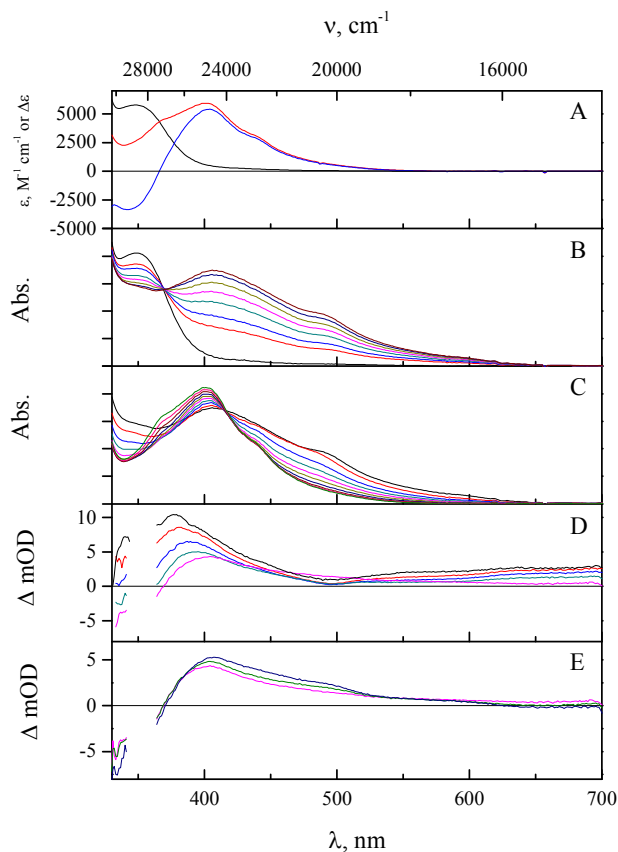


Figure 4. UV-visible and transient absorption spectra in 1,2-dichloroethane (DCE). A) Electronic spectra of S,S-[Ru(bpy)<sub>2</sub>(bpSOp)]<sup>2+</sup> (black), bulk photolysis product S,O-[Ru(bpy)<sub>2</sub>(bpSOp)]<sup>2+</sup> (red), and difference (photoproduct – S,S) (blue). B) UV-visible spectra from bulk photolysis obtained sequentially at 0 (black, S,S-isomer), 1, 2, 4, 6, 9, 14 and 24 min (dark red). C) UV-visible spectra from bulk photolysis obtained sequentially at 24 (dark blue) 165, 265, 360, 460, 530, 605, 700, 820, and 995 min (dark green). D) Transient absorption spectra obtained from pump–probe delays of 0.5 (black), 1 (red), 2 (blue), 5 (teal) and 35 (magenta) ps. E) Transient absorption spectra obtained from pump–probe delays of 35 (magenta), 75 (green) and 500 (dark blue) ps.

### C. Thermal and Photochemical Reversion.

Reversion of the photoproduct from bulk photolysis of [Ru(bpy)<sub>2</sub>(bpSOp)]<sup>2+</sup> to the S,O- and S,S-isomers was monitored by UV-visible spectroscopy. The kinetic behavior is strikingly solvent dependent, as suggested by the bulk photolysis data discussed above. In propylene carbonate, thermal reversion of the O,O-isomer at room temperature clearly exhibits two distinct kinetic phases. Both phases are characterized by loss of absorption at 350 and 500 nm (indicative of the O,O-isomer) and increased absorption about 405 nm (ascribed to an S,O-isomer). An early isosbestic point is observed at 430 nm and migrates to 447 nm at later times, while another isosbestic point is observed at 378 nm throughout the experiment. By monitoring the change in absorption as a function of time at the late- and early-forming isosbestic points, we have determined thermal reversion rates for both a rapid and a slow transformation (Figures S11 and S12). The spectral changes observed in the time regime of the more rapid rate,  $4.68 \times 10^{-4} \text{ s}^{-1}$ , are consistent with formation of an S,O-bonded

isomer from an O,O-bonded isomer. Thus, this rate is assigned to thermally-induced formation of an S,O-bonded isomer from an O,O-bonded isomer on the ground state potential energy surface. The spectral features observed during the slower kinetic component,  $9.79 \times 10^{-6} \text{ s}^{-1}$ , are also consistent with the thermal formation of an S,O-bonded isomer from an O,O-bonded isomer. As two isomers are observed in the  $^1\text{H}$  NMR spectrum of ground state  $\text{S,S-}[\text{Ru}(\text{bpy})_2(\text{bpSOp})]^{2+}$ , it seems reasonable to expect two distinct conformational O,O-isomers in the photoproduct. We assign the two distinct kinetic phases in the thermal reversion data to a S $\rightarrow$ O isomerization in each conformation. Indeed, we have observed similar, multi-phase kinetics in the thermal reversion of  $[\text{Ru}(\text{bpy})_2(\text{OSO})]^+$  (OSO is 2-methylsulfinylbenzoate),<sup>40, 41</sup> where DFT calculations indicated that the observed behavior is a consequence of two O-bonded isomers produced upon irradiation of the S-bonded complex.<sup>42, 43</sup> Formation of the S,S-isomer of  $[\text{Ru}(\text{bpy})_2(\text{bpSOp})]^{2+}$  occurs more slowly, on a timescale of weeks.

Thermal reversion of the photoproduct from irradiation of S,S- $[\text{Ru}(\text{bpy})_2(\text{bpSOp})]^{2+}$  in DCE (such that both the S,O- and O,O-bonded isomeric species are present) demonstrates spectral features consistent with reversion from a mixture including both S,O- and O,O-isomers to one featuring only the S,O-isomer. As in propylene carbonate, two thermal reversion rates at room temperature are observed by monitoring the UV-vis spectra (Figure S13). Both thermal isomerization rates,  $2.41 \times 10^{-3}$  and  $4.39 \times 10^{-5} \text{ s}^{-1}$ , are an order of magnitude faster than their respective fast and slow counterparts in propylene carbonate. While we do not expect this effect to be due to differences in driving force for the two solvents, additional studies must be performed to learn the origin of this effect.

Notably, irradiation of O,O- $[\text{Ru}(\text{bpy})_2(\text{bpSOp})]^{2+}$  in propylene carbonate or dichloroethane at 532 nm yields a more rapid loss of the O,O-bonded species in comparison to the respective thermal reversion data. Continuous irradiation of each solution ultimately yields a spectrum consistent with that assigned to the S,O-bonded complex. This observation suggests a photochemical pathway for reversion from the O,O-bonded isomer in both solvents. By monitoring the loss of the O,O-bonded species, and accounting for the thermal reversion rate of the O,O-bonded isomer, a photochemical quantum yield of 0.019 (0.002) has been determined in PC, and 0.0013 (0.0001) in DCE. In both cases, continuous irradiation at 532 nm yields only the absorption spectrum of an S,O-bonded isomer, and no photochemical pathway to the S,S-bonded isomer is observed. Given the very low quantum yields for the O,O $\rightarrow$ S,O isomerization at direct MLCT irradiation, it is apparent that the photostationary state observed in DCE is a consequence of the rapid thermal reversion rate, which is greater than both the DCE S,O $\rightarrow$ O,O quantum yield and O,O $\rightarrow$ S,O quantum yield. For propylene carbonate, the photostationary state spectrum represents primarily the O,O isomer as both the thermal and photochemical reactions to produce the S,O isomer are comparatively slow.

#### D. Pump-Probe Time-Resolved Absorption Spectroscopy.

Ultrafast transient absorption spectroscopy studies were performed in PC and DCE to gain insight into the excited state and isomerization dynamics of  $\text{S,S-}[\text{Ru}(\text{bpy})_2(\text{bpSOp})]^{2+}$ . In propylene carbonate, 355 nm excitation yields an initial excited state spectrum at 0.60 ps characterized by an intense positive absorption about 375 nm and a less intense broad absorption near 500 nm which extends past 650 nm (Figure 3d). Consistent with the canonical assignment of ultrafast relaxation dynamics in ruthenium polypyridyl complexes, the defined band ( $\sim 375$  nm) is assigned to an absorption arising from reduced bpy  $\pi^* \rightarrow \pi^*$  transitions, while the largely featureless, low energy absorption is attributed to ligand-to-metal charge transfer (LMCT) transitions from the unreduced bpy  $\pi \rightarrow \text{Ru(III)} \text{ d}\pi$ , with contributions from additional low energy  $\pi^* \rightarrow \pi^*$  transitions of the reduced bpy.<sup>31</sup> Over the next 30 ps, the well-defined absorption at 375 nm reduces in intensity and a mild bathochromic shift to 400 nm is observed. The low energy absorption also reduces in intensity. At longer times (Figure 3E,  $t > 35$  ps), the 400 nm band grows slightly in intensity and continues to shift to 405 nm. A distinct bleach is apparent blue of 360 nm (laser pulse notwithstanding), consistent with the loss of the MLCT absorption belonging to the S,S-bonded complex. Moreover, the excited state features red of 600 nm decay to zero, indicating deactivation of the  $^3\text{MLCT}$  excited state and, accordingly, formation of the photoproduct coincident with the ground state (S,S-bonded) isomer. Positive absorption is observed about 500 nm in the form of a broad, poorly defined band. The spectrum observed at 1000 ps persists through the end of the experiment ( $\sim 3$  ns). The 405 nm absorption is reminiscent of the distinct S,O-bonded complex observed as an intermediate in the bulk photolysis spectra, and the newly formed ground state complex is assigned thusly. The broad absorption feature about 500 nm is further suggestive of the absorption spectrum of the O,O-bonded isomer. Indeed, we have recently reported the experimental observation of two isomerizations following single photon absorption in a bis-sulfoxide complex.<sup>31</sup> The breadth of the newly formed ground state features (extending to  $\sim 600$  nm) and general band shape about 500 nm suggest that some O,O-bonded isomer is also produced by a single photon absorption in this case.

Single wavelength kinetics were fit to determine the observed time constants of excited state relaxation and isomerization. The kinetic fits collected at 410 and 615 nm report on dynamics of the excited state and formation of photoproducts. The fit observed at 521 nm lies at a late-forming isosbestic point and so describes excited state dynamics, but does not relay information regarding isomerization itself. Time constants are compiled in Table 3, and in aggregate reveal three distinct time components,  $\sim 0.2$ , 2 and 96 ps. The shortest time component is assigned to formation of the  $^3\text{MLCT}_{\text{SS}}$ , based on ultrafast studies of transition metal polypyridine complexes. The intermediate time component (2 ps) is ascribed to vibrational cooling of the  $^3\text{MLCT}$  state. We propose that the triplet excited state ( $^3\text{ES}$ ) surface is both MLCT and metal-centered (MC) in

nature and exhibits a nuclear conformation poised for isomerization. The longest time constant, 96 ps, describes relaxation from  $^3\text{ES}$  concomitant with the formation of new ground state absorption features. Consequently, this time constant includes formation of the S,O-bonded ground state isomer. As a new absorption is observed at 500 nm, consistent with the O,O-bonded isomer, this time constant also represents formation of the *bis*-O-bonded photoproduct from the excited state. Global fitting analysis yields three time constants, of 0.18 (0.04), 2.8 (0.4) and 95 (11) ps, which are in good agreement with the single-wavelength kinetics observed. As stated above, spectral overlap of the three isomers and rapid formation of the O,O-bonded species from the S,O-isomer prevents the determination of the S,S- to S,O-isomer and S,O- to O,O-isomer quantum yields, as we cannot independently monitor the concentration of each species as a function of light absorbed per unit time. The aggregate quantum yield of the formation of photoproduct is determined to be 0.42(5). Based on this value (and global fitting data), an isomerization time constant of 229 ps is found.

Table 3. Time constants for excited state processes from single wavelength and global fitting analysis for  $[\text{Ru}(\text{bpy})_2(\text{bpSO})]^{2+}$  in DCE and PC.

|       | 1,2-Dichloroethane<br>( $\Phi = 0.57(2)$ ) | Propylene Carbonate<br>( $\Phi = 0.42(5)$ ) |
|-------|--|---|
|       | <b>470 nm</b>                              | <b>410 nm</b>                               |
| $t_1$ | $0.14 \pm 0.07$                            | $0.2$ (fixed)                               |
| $t_2$ | $1.0 \pm 0.3$                              | $6.3 \pm 1.1$                               |
| $t_3$ | $44.4 \pm 1.7$                             | $82.0 \pm 10.2$                             |
|       | <b>582 nm</b>                              | <b>521 nm</b>                               |
| $t_1$ | $0.13 \pm 0.03$                            | $0.33 \pm 0.1$                              |
| $t_2$ | $1.11 \pm 0.06$                            | $1.7 \pm 0.9$                               |
|       | <b>625 nm</b>                              | <b>615 nm</b>                               |
| $t_1$ | $1.9 \pm 0.2$                              | $0.15 \pm 0.05$                             |
| $t_2$ | $39.3 \pm 4.7$                             | $2.68 \pm 0.4$                              |
| $t_3$ | -  | $103.1 \pm 15$                              |
|       | <b>Global Fitting Analysis</b>             | <b>Global Fitting Analysis</b>              |
| $t_1$ | $0.1$ (fixed)                              | $0.19 \pm 0.04$                             |
| $t_2$ | $2.3 \pm 0.5$                              | $2.8 \pm 0.4$                               |
| $t_3$ | $52.0 \pm 10.5$                            | $95.6 \pm 11$                               |

The spectral features of the femtosecond transient absorption experiment in DCE are qualitatively similar to those observed in propylene carbonate (Figure 4D, 4E). The excited state formed by 355 nm irradiation yields characteristic transitions from the reduced bpy (380 nm) and LMCT transitions ( $> 500$  nm), which grow in intensity for  $\sim 500$  fs. Over the subsequent 35 ps, the band at 380 nm shifts to 400 nm, and the broad, featureless absorption of the LMCT decays at  $\lambda > 550$  nm. Between 35 and 100 ps the excited state absorption past 600 nm decays to zero, and the peak at 400 nm continues to shift to 405 nm and grow in intensity. The spectrum at 100 ps essentially persists to the end of the experiment with additional broadening and shifting of the peak maximum to lower energy. These observations are consistent with formation of a ground state isomer and vibrational relaxation on the ground state potential energy surface. As in the PC experiment, the new ground state absorption at 405 nm is assigned to the S,O-bonded isomer, while the band at 500 nm is contributed by the O,O-bonded isomer.

Global fitting and single wavelength kinetics have been analyzed to describe the excited state dynamics of  $[\text{Ru}(\text{bpy})_2(\text{bpSO})]^{2+}$  in DCE. A triexponential fit is observed in the global fitting analysis, with time constants of 0.1 (fixed), 2.3 (0.5) and 52.0 (10.5) ps. The most rapid of these time constants is fixed at 0.1 ps, based on findings from the single wavelength analysis, and is assigned to formation of an initial  $^3\text{MLCT}$  state formed from the singlet excited state. The intermediate time component, 2 ps, is attributed to vibrational cooling and early structural rearrangements, as described above. The longest time component of 90.8 ps, is assigned to formation of the ground and metastable state isomers, namely, relaxation to the S,S-, S,O- and O,O-bonded ground states. Single wavelength kinetics were obtained at 470, 582 and 625 nm and are in good accord with the global fit results. Time constants at these wavelengths are summarized in Table 3. Assuming isomerization occurs from the  $^3\text{ES}$  surface and in conjunction with the quantum yield of isomerization,  $\tau_{\text{S} \rightarrow \text{O}}$  of 91 ps is found.

### E. Isomerization in Related Compounds

A comparison of the structural characteristics of  $[\text{Ru}(\text{bpy})_2(\text{bpSO})]^{2+}$  and other reported photochromic polypyridyl ruthenium sulfoxide complexes anticipates aspects of the photochemistry displayed by this molecule. Of particular note are the Ru-S bond distances and S-Ru-S chelate bite angles found in the crystal structure. The complex  $[\text{Ru}(\text{bpy})_2(\text{bpSO})]^{2+}$  is a useful analogue because bpSO is the five-membered chelate version of bpSO, while OSSO is a six-membered chelate. In  $[\text{Ru}(\text{bpy})_2(\text{bpSO})]^{2+}$ , the Ru-S bond distance lies between those observed in  $[\text{Ru}(\text{bpy})_2(\text{bpSO})]^{2+}$  (shortest) and  $[\text{Ru}(\text{bpy})_2(\text{OSSO})]^{2+}$  (longest). Similarly, the chelate bite angle in  $[\text{Ru}(\text{bpy})_2(\text{bpSO})]^{2+}$  is intermediate to  $[\text{Ru}(\text{bpy})_2(\text{bpSO})]^{2+}$  (most acute) and  $[\text{Ru}(\text{bpy})_2(\text{OSSO})]^{2+}$  (most obtuse). As this angle is a direct consequence of the orbital overlap and Ru-S bond distances in these molecules, it is tempting to draw correlations between it and photochemical reactivity. In the series  $[\text{Ru}(\text{bpy})_2(\text{bpSO})]^{2+}$ ,  $[\text{Ru}(\text{bpy})_2(\text{bpSO})]^{2+}$  and  $[\text{Ru}(\text{bpy})_2(\text{OSSO})]^{2+}$ , there is no formation of an O,O-bonded species in the bpSO complex, a mild contribution in the bpSO complex and substantial formation of in the OSSO complex, upon single photon absorption of the S,S-bonded isomer.<sup>31, 32</sup> This series reflects the trend in increasing Ru-S bond distance, as well as increasing S-Ru-S chelate bite angle. Beyond the bond distances and angles, it is surprising that such a seemingly small substitution in the chelate bridge between  $[\text{Ru}(\text{bpy})_2(\text{bpSO})]^{2+}$  and  $[\text{Ru}(\text{bpy})_2(\text{OSSO})]^{2+}$  ( $\text{CH}_2$  for  $\text{Si}(\text{Me})_2$ ) results in such a dramatic change in comparing their photochemical reactivities. In analogy, it is worth noting the smaller rotational barrier for methylsilane ( $1.7 \text{ kcal mol}^{-1}$ ) relative to ethane ( $2.9 \text{ kcal mol}^{-1}$ ) brought about by the longer C-Si bond, which reduces repulsive interactions in the eclipsed conformation. The S $\rightarrow$ O isomerizations in  $[\text{Ru}(\text{bpy})_2(\text{bpSO})]^{2+}$  and  $[\text{Ru}(\text{bpy})_2(\text{OSSO})]^{2+}$  must involve some rotation and displacement of the methylene group  $\alpha$  to the sulfoxide moiety. A lowered rotational barrier in the silane-

bridged ligand may facilitate isomerization. As such, our laboratory is presently investigating this effect on photochemical isomerization.

## Conclusions

Unique behavior has been described in the excited and ground state isomerizations of  $[\text{Ru}(\text{bpy})_2(\text{bpSO})]^{2+}$ . The thermal reversion rates in DCE are greater than those in PC, and this difference is attributed to stabilization of the transition state in DCE. In turn, this change in the thermal reversion rate contributes to the differing product distributions that comprise the photostationary state in either solvent. Furthermore, the extension of the chelate bridge to a six-membered ring in the ground state isomer apparently permits isomerization including formation of the O,O-bonded isomer directly from the S,S-bonded isomer, in comparison to the five-membered chelate analogue. Thus, our study of  $[\text{Ru}(\text{bpy})_2(\text{bpSO})]^{2+}$  demonstrates that the reactivity of *bis*-sulfoxide complexes is sensitive to small changes in structure. In comparison to the five-membered chelate analogue,  $[\text{Ru}(\text{bpy})_2(\text{bpSO})]^{2+}$ , the six-membered chelate complex  $[\text{Ru}(\text{bpy})_2(\text{bpSO})]^{2+}$  features similar photoisomerization rates, but the structural modification appears to activate an excited state pathway which accesses the O,O-bonded isomer. Comparison to the analogous six-membered chelate  $[\text{Ru}(\text{bpy})_2(\text{OSSO})]^{2+}$ , however, implies that greater flexibility is necessary to more substantially activate such a pathway. By investigating the connections between structure and solvent on photochemical reactivity, we will be able to further our understanding of the coupling of nuclear motion during excited state processes. Such information will lead the design and construction of more effective photochromic compounds and materials for specific applications ranging from information storage to energy conversion.

## Acknowledgements

This material is based upon work supported by the National Science Foundation under Grants CHE 0809699, 0947031, and 1112250. JPM recognizes the Honor's Tutorial College (HTC) at Ohio University for funding through the Provost's Undergraduate Research Fund (PURF).

## Notes and references

<sup>a</sup> Department of Chemistry and Biochemistry, Nanoscale and Quantum Phenomena Institute, Ohio University, Clipping Laboratories, Athens, OH 45701, USA

<sup>b</sup> Department of Chemistry, Knight Chemical Laboratory, University of Akron, Akron, Ohio 44325, USA

† Electronic Supplementary Information (ESI) available: CCDC-1002146 and 1002147 contain the supplementary crystallographic data for this paper for compounds  $[\text{Ru}(\text{bpy})_2(\text{bptp})](\text{PF}_6)_2$  and  $[\text{Ru}(\text{bpy})_2(\text{bpSO})](\text{BF}_4)_2$ . This data can be obtained free of charge from the Cambridge Crystallographic Data Center via [www.ccdc.cam.ac.uk/data\\_request/cif](http://www.ccdc.cam.ac.uk/data_request/cif). See DOI: 10.1039/b000000x/

- M. J. Bearpark, M. Boggio-Pasqua, M. A. Robb and R. Ogliaro, *Theor. Chem. Acc.*, 2006, **116**, 670-682.
- M. Boggio-Pasqua, M. J. Bearpark, P. A. Hunt and M. A. Robb, *J. Am. Chem. Soc.*, 2002, **124**, 1456-1470.
- M. Boggio-Pasqua, M. J. Bearpark and M. A. Robb, *J. Org. Chem.*, 2007, **72**, 4497-4503.
- M. Boggio-Pasqua, M. Ravaglia, M. J. Bearpark, M. Garavelli and M. A. Robb, *J. Phys. Chem. A*, 2003, **107**, 11139-11152.
- M. A. Robb, F. Bernardi and M. Olivucci, *Pure Appl. Chem.*, 1995, **67**, 783-789.
- M. Sanchez-Lozano, C. M. Estevez, J. Hermida-Ramon and L. Serrano-Andres, *J. Phys. Chem. A*, 2011, **115**, 9128-9138.
- B. G. Levine and T. J. Martinez, *Ann. Rev. Phys. Chem.*, 2007, **58**, 613-634.
- T. J. Martinez, *Nature*, 2010, **467**, 412-413.
- S. Matsika and P. Krause, *Ann. Rev. Phys. Chem.*, 2011, **62**, 621-643.
- D. R. Yarkony, *Acc. Chem. Res.*, 1998, **31**, 511-518.
- D. Schaniel, M. Imlau, T. Weisemoeller, T. Woike, K. W. Krämer and H.-U. Güdel, *Adv. Mater.*, 2007, **19**, 723-726.
- M. Imlau, T. Woike, R. Schieder and R. A. Rupp, *Phys. Rev. Lett.*, 1999, **82**, 2860-2863.
- A. M. Kolpak and J. C. Grossman, *Nano. Lett.*, 2011, **11**, 3156-3162.
- T. J. Kucharski, Y. Tian, S. Akbulatov and R. Boulatov, *Energy Environ. Sci.*, 2011, **4**, 4449-4472.
- K. Moth-Poulsen, D. Čoso, K. Börjesson, N. Vinokurov, S. K. Meier, A. Majumdar, K. P. C. Vollhardt and R. A. Segalman, *Energy Environ. Sci.*, 2012, **5**, 8534-8537.
- R. Boese, J. K. Cammack, A. J. Matzger, K. Pflug, W. B. Tolman, K. P. C. Vollhardt and T. W. Weidman, *J. Am. Chem. Soc.*, 1997, **119**, 6757-6773.
- Y. Kanai, V. Srinivasan, S. K. Meier, K. P. C. Vollhardt and J. C. Grossman, *Angew. Chem. Int. Ed.*, 2010, **49**, 8926-8929.
- E. Orgiu and P. Samori, *Adv. Mater.*, 2014, **26**, 1827-1845.
- M.-M. Russew and S. Hecht, *Adv. Mater.*, 2010, **22**, 3348-3360.
- J. Zhang, Q. Zou and H. Tian, *Adv. Mater.*, 2013, **25**, 378-399.
- M. Morimoto and M. Irie, *J. Am. Chem. Soc.*, 2010, **132**, 14172-14178.
- F. Terao, M. Morimoto and M. Irie, *Angew. Chem. Int. Ed.*, 2012, **51**, 901-904.
- T. Kim, L. Y. Zhu, R. O. Al-Kaysi and C. J. Bardeen, *Chem. Phys. Chem.*, 2014, **15**, 400-414.
- K. M. Lee, D. H. Wang, H. Koerner, R. A. Vaia, L. S. Tan and T. J. White, *Macromol. Chem. Phys.*, 2013, **214**, 1189-1194.
- A. Priimagi, A. Shimamura, M. Kondo, T. Hiraoka, S. Kubo, J.-I. Mamiya, M. Kinoshita, T. Ikeda and A. Shishido, *ACS Macro Lett.*, 2012, **1**, 96-99.
- Y. Jin, S. I. M. Paris and J. J. Rack, *Adv. Mater.*, 2011, **23**, 4312-4317.
- Photochromism Molecules and Systems*, Elsevier, Amsterdam, The Netherlands, 2003.
- B. A. McClure and J. J. Rack, *Eur. J. Inorg. Chem.*, 2010, 3895-3904.
- J. J. Rack, *Z. Kristallogr.*, 2008, **223**, 356-362.
- J. J. Rack, *Coord. Chem. Rev.*, 2009, **253**, 78-85.
- K. Garg, A. W. King and J. J. Rack, *J. Am. Chem. Soc.*, 2014, **136**, 1856-1863.

32. A. W. King, Y. Jin, J. T. Engle, C. J. Ziegler and J. J. Rack, *Inorg. Chem.*, 2013, **52**, 2086-2093.
33. N. V. Mockus, D. Rabinovich, J. L. Petersen and J. J. Rack, *Angew. Chem. Int. Ed.*, 2008, **47**, 1458-1461.
34. B. P. Sullivan, D. J. Salmon and T. J. Meyer, *Inorg. Chem.*, 1979, **17**, 3334-3341.
35. J.-P. Collin, D. Jouvenot, M. Koizumi and J.-P. Sauvage, *Inorg. Chim. Acta*, 2007, **360**, 923-930.
36. M. K. Smith, J. A. Gibson, C. G. Young, J. A. Broomhead, P. C. Junk and F. R. Keene, *Eur. J. Inorg. Chem.*, 2000, 1365-1370.
37. J. C. Dobson and T. J. Meyer, *Inorg. Chem.*, 1988, **27**, 3283-3291.
38. J. J. Rack and N. V. Mockus, *Inorg. Chem.*, 2003, **42**, 5792-5794.
39. N. V. Mockus, J. L. Petersen and J. J. Rack, *Inorg. Chem.*, 2006, **45**, 8-10.
40. D. P. Butcher Jr., A. A. Rachford, J. L. Petersen and J. J. Rack, *Inorg. Chem.*, 2006, **45**, 9178-9180.
41. V. Dieckman, S. Eicke, J. J. Rack, T. Woike and M. Imlau, *Opt. Exp.*, 2009, **17**, 15052-15060.
42. A. J. Gottle, I. M. Dixon, F. Alary, J. L. Heully and M. Boggio-Pasqua, *J. Am. Chem. Soc.*, 2011, **133**, 9172-9174.
43. B. A. McClure, N. V. Mockus, D. P. Butcher, D. A. Lutterman, C. Turro, J. L. Petersen and J. J. Rack, *Inorg. Chem.*, 2009, **48**, 8084-8091.

TOC Figure

